EES Solar

PAPER

View Article Online
View Journal

Cite this: DOI: 10.1039/d5el00204d

From precursor to performance: the impact of FAI impurities on halide perovskite thin films and devices

Siyu Yan, Saqlain Choudhary, Emily A. Hudson, Ruohan Zhao, Henry J. Snaith, Michael B. Johnston and Nakita K. Noel *

While metal halide perovskites have yielded remarkable power conversion efficiencies in photovoltaic applications, uncertainty concerning their long-term stability remains a significant barrier to widespread deployment. Previous studies have demonstrated that trace impurities present in perovskite precursor materials can influence the crystallisation dynamics of perovskite thin-films and hence, affect crystal structure, film morphology and optoelectronic properties. However, the nature of the impurities in formamidinium iodide (FAI) and their effect(s) on film quality and device performance remain underexplored. In this work, we carry out a detailed analysis of the impurities present in commonly used commercial FAI sources, and probe their impact on the composition, structure, and optoelectronic quality of the resulting perovskite thin-films and devices. We find that while some FAI impurities can improve the optoelectronic properties of solution-processed perovskite thin-films, in vapour-processed films, their presence alters the sublimation behaviour of FAI, favouring irreversible degradation pathways which lead to the formation of *sym*-triazine. While *sym*-triazine does not directly incorporate into the perovskite films, the impurity-driven variation in sublimation behaviour results in films which can deviate from the target stoichiometry, even under otherwise optimised conditions; and thus, do not fully convert into the desired photoactive phase, eventually causing poor material stability. Our results highlight the importance of understanding and controlling impurity concentrations in perovskite precursor materials as a route to enhancing both performance and process reproducibility in perovskite solar cells.

Received 7th December 2025
Accepted 10th April 2026

DOI: 10.1039/d5el00204d

rsc.li/EESSolar

Broader context

In just over a decade, halide perovskites have become the most promising emerging thin-film solar technology. One major advantage of these materials has been the ability to deposit high-quality films through different processing techniques such as solution-based or vapour phase approaches. As perovskite solar cells move ever closer to commercial market entry and large-scale deployment, it is becoming increasingly important to focus on high-volume reproducibility and long-term stability. While lead halide perovskites are generally considered highly defect tolerant, meaning that their initial solar cell performances may not be impeded by lattice defects, there is mounting evidence that these initially hidden defects and impurities may in fact have quite detrimental impacts on the long-term reliability of the absorber. The concentration of such impurities is often determined by a key, but often overlooked, factor which is the purity of the precursor materials used in the fabrication of perovskite thin films. In this work we probe the impacts of precursor impurities in solution and vapour processing by systematically identifying and evaluating the impurities found in commercial FAI sources. We find that the nature of the impurities has highly diverging effects on the film quality and composition depending on the deposition technique. These findings underscore the importance of precursor-quality control and offer new opportunities for improving the reliability and scalability of perovskite solar cell manufacturing.

At present, next-generation solar cells based on metal halide perovskite (MHP) semiconductors have already achieved promising certified power conversion efficiencies (PCEs) of up to 27.3% in single-junction devices, and 35.0% in Si/perovskite tandem devices.[1] While the rapid increase in the efficiency of these devices is partly due to the excellent intrinsic optoelectronic properties of MHPs,[2–4] significant performance gains have been made as a result of improving the crystallinity and optoelectronic quality of perovskite thin films. These improvements have largely been made through advances in process engineering, compositional alloying, solvent and additive engineering in precursor inks, and various interface passivation techniques.[5–9] Notably, it has been observed that precisely controlling crystallisation kinetics is crucial to achieving efficient and stable perovskite solar cells (PSCs).[10–12]

One underexplored area of research is the impact of trace precursor impurities on the optoelectronic properties and long-term stability of perovskite films. In the vast majority of published literature, perovskite precursor materials (lead iodide

Department of Physics, University of Oxford, Clarendon Laboratory, Parks Road, Oxford OX1 3PU, UK. E-mail: nakita.noel@physics.ox.ac.uk

(PbI_2), formamidinium iodide (FAI) *etc.*) are usually used as-received, without further purification. However, recent reports suggest that there can be impurities present in these precursors which modulate the crystallisation process, and can have competing effects based on the nature and concentration of the impurities.[13–19] For example, Kerner *et al.* characterised five commercially available PbI_2 materials and found that one PbI_2 source contained higher concentrations of a lead acetate trihydrate ($Pb[OAc]_2 \cdot 3H_2O$) impurity which had a negative effect on perovskite solar cell performance, while another PbI_2 source contained potassium iodide (KI), which resulted in higher quality films and improved device performance.[20] Given that precursor materials can contain a variety of different impurities which may have beneficial and/or detrimental effects on devices, it stands to reason that a thorough understanding, and subsequent fine control, of which impurities precursors contain can be beneficial to perovskite film quality, device performance, long-term stability, and potentially even batch-to-batch reproducibility.

Another point which should be considered here, is that the presence of impurities in perovskite precursors may have different effects based on whether the perovskite films are fabricated using solution-based or vapour-based deposition techniques. Borchert *et al.* have previously investigated the impact of organic precursor impurities on the quality of methylammonium lead triiodide ($MAPbI_3$) films deposited through thermal vapour deposition.[21] It was found that while the presence of phosphorus-based impurities had a negligible impact on device performance, it did significantly affect the consistency of the evaporation rate. Conversely, research probing the impact of these phosphorus-based impurities in spin-coated perovskite solar cells showed an improvement in device performance, as a result of changing the crystallisation dynamics of the perovskite thin-film.[22,23] This suggests that precursor impurities may play very different roles in 'dry' deposition processes than they do in solvent-mediated ones.

Currently, a significant portion of research into perovskite solar cells is focused on formamidinium-based perovskites due, in part, to their superior thermal and chemical stability, as compared to their MA-based counterparts.[24–26] In comparison to MAI, another advantage of FAI is that it yields a more controllable, and significantly more consistent deposition rate.[27–29] However, during the thermal evaporation of FAI, Kroll *et al.* detected a variety of degradation products using mass spectrometry. Of particular note here, was the detection of *sym*-triazine (a product of the irreversible decomposition of FAI) at a lower temperature (50 °C to 120 °C) than the sublimation temperature of FAI (above 125 °C).[30]

This raises questions as to if (and how) impurities present in FAI can on one hand, affect not only its decomposition temperature, but the composition and stability of vapour-deposited perovskite films, and on the other, what (if any) is the impact of these impurities on solution-processed films and devices. Herein, we seek to address two questions: (i) what are the initial impurities in FAI and how do they impact film formation and thin-film properties in halide perovskites?; and (ii) do they have unique effects depending on whether films are solution-processed or vapour-processed?

We first identify the impurities in as-received FAI *via* nuclear magnetic resonance (NMR) measurements. Through a simple recrystallisation procedure, we purify the as-received FAI with the goal of removing the impurities identified. By comparing perovskite films fabricated with the as-received and recrystallised FAI, we probe the direct impact of these impurities, and show that their presence impacts the optoelectronic properties of both solution- and vapour-processed MHP films, hence affecting device performance. Curiously, we find that certain impurities in the FAI can have beneficial effects on the optoelectronic properties of the MHP thin film. However, this is only the case for the solution-processed films. In the case of vapour-processed films, these impurities have detrimental effects. Here, we identify the underlying mechanism to be changes in the sublimation behaviour of FAI which leads to increased formation of *sym*-triazine. Although volatile degradation products are not incorporated into the films, altered sublimation behaviour can still induce stoichiometric deviations, even under optimised conditions, promoting the formation of unwanted, lower symmetry, polytype phases. The existence of these non-photoactive polytype phases impairs device performance, and can be correlated with reduced material stability. Our results highlight the importance of understanding the role of precursor impurities in the crystallisation of MHP thin films.

Impurity analysis in formamidinium iodide

To understand the impact of FAI impurities on perovskite films and devices, we must first screen for and identify potential impurities, and determine whether they can be removed through simple purification techniques such as recrystallisation. To probe this, we conduct proton nuclear magnetic resonance (^{1}H NMR) experiments on as-received and recrystallised (see SI for details) FAI obtained from a commonly used supplier and show the results in Fig. 1. In Fig. 1a, we see that both the as-received and recrystallised FAI show the characteristic peaks [CH group at 8.32 ppm (singlet), and amine groups at 9.26 ppm (singlet)] of FA^+. However, we observe distinct spectral differences in the range of 1 to 4.5 ppm (Fig. 1b). For the as-received FAI, we see signals associated with ethyl acetate [δ 1.19 ppm (triplet), δ 2.01 ppm (singlet), δ 4.05 ppm (quartet)], ethanol [δ 1.10 ppm (triplet), δ 3.40 ppm (quartet)], and isopropanol [δ 1.08 ppm (doublet), δ 3.88 ppm (septet)]. These impurities are likely to be residual solvents from the synthesis and/or purification of FAI. After recrystallisation, these peaks are no longer present in the ^{1}H NMR spectrum. Instead, we observe a signal in this range which we attribute to diethyl ether [δ 1.10 ppm (triplet), δ 3.54 ppm (quartet)], the solvent which was used to wash the recrystallised product. To exclude the possibility that the presence of these impurities in the as-received FAI is simply a batch anomaly, we obtain and test samples from another batch number from supplier A, along with a sample from supplier B. (Fig. S1). ^{1}H NMR results confirm that both batches

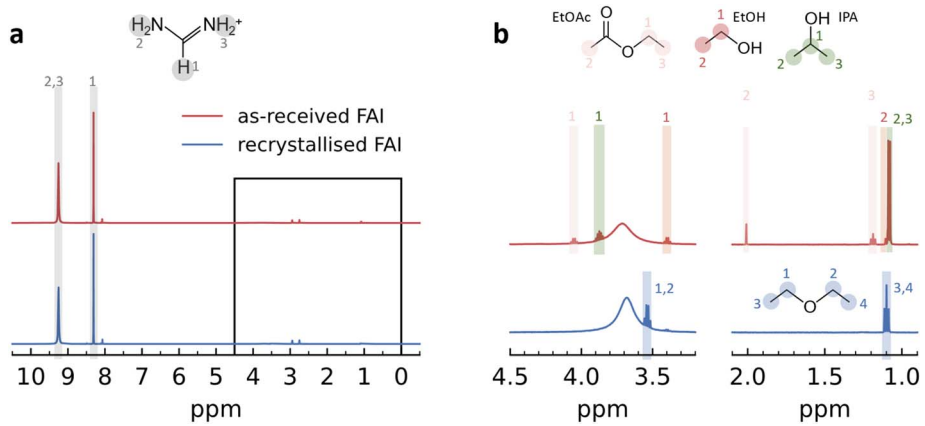

Fig. 1 Solution ^{1}H NMR spectra of as-received FAI and recrystallised FAI dissolved in DMF-d_7. (a) ^{1}H NMR spectrum of as-received FAI and recrystallised FAI. In both cases, the main peaks can be attributed to the protons of the methine [CH (1)] and amine [NH_2 (2, 3)] groups of formamidinium. (b) Low ppm region of ^{1}H NMR spectra of as-received and recrystallised FAI. In as-received FAI, we observe signals from ethyl acetate (EtOAc), ethanol (EtOH) and isopropanol (IPA), whereas in recrystallised FAI, we observe only a signal from diethyl ether.

of as-received FAI (from supplier A) contain the same types of impurities, which we can effectively remove through simple recrystallisation processes.

Influence of FAI impurities on solution-processed MHP films and devices

Having established the nature of the organic impurities in FAI from supplier A, we proceed to investigate the impact of these impurities on the structural and optoelectronic properties of solution-processed perovskite thin films and devices. For convenience, solution-processed MHP films of composition $FA_{0.83}Cs_{0.17}Pb(I_{0.8}Br_{0.2})_3$ which are fabricated using as-received and recrystallised FAI are abbreviated as 'ctrl-S' and 'rextal-S' respectively. We observe a negligible difference in the absorption coefficient (Fig. 2a and S2) and X-ray diffraction (XRD) patterns (Fig. S3) for ctrl-S and rextal-S films, which indicates that removing the impurities in FAI neither changes the structure nor composition of solution-processed MHP films. However, we note that there is a significant quenching of the steady-state photoluminescence (PL) accompanied by a reduction of the charge-carrier lifetime (Fig. 2b and S4) in rextal-S films. This indicates an increase in non-radiative recombination of charge carriers as a result of the removal of the organic impurities in FAI. Hence, it appears that in solution processing, these impurities yield films with fewer electronic defects, either through modulating ink chemistry or altering crystallisation kinetics.

To investigate whether this improvement in optoelectronic properties will translate into enhanced solar-cell performance, we incorporate these films into photovoltaic devices (Fig. 2c). Here, for devices fabricated using rextal-S films (solution-processed MHP films using recrystalised FAI) we see a drop across all performance parameters, resulting in a reduction of the average PCE from 18.3 ± 0.3% to 16.4 ± 1.8% accompanied by a much broader distribution in performance (Fig. 2d and Table S1). We observe similar trends in devices made across different batches (Fig. S5, S6 and S7). The large reduction in the average PCE for devices fabricated with rextal-S films is primarily due to a substantial decrease in both the open-circuit voltage (V_{oc}) and fill factor (FF) (Fig. S8 and S9). To verify that the observed decrease in device performance is indeed due to the removal of impurities from as-received FAI (supplier A), we first make devices with high-purity FAI available from supplier B (details in SI) as a means of excluding the possible influence of diethyl ether in the recrystallised FAI. We find that devices fabricated using recrystallised FAI (supplier A) and high-purity FAI (supplier B) achieve comparable efficiencies (see Fig. S10). This confirms the negligible influence of diethyl ether in recrystallised FAI on the device performance. Nonetheless, we note that these devices are both outperformed by those made using as-received FAI (supplier A). This supports our hypothesis that the organic impurities present in FAI from supplier A improve the performance of perovskite films and devices.

Given that ethyl acetate and alcohols (isopropanol and ethanol) are two main impurities identified in as-received FAI (supplier A), to determine which impurity/impurities are responsible for the improved device performance, we individually add different amounts of ethyl acetate and isopropanol to the perovskite precursor ink made using recrystallised FAI. When 1 vol% ethyl acetate is added to the precursor ink, the device performance is enhanced as a result of increased V_{oc} and FF (Fig. S11). Interestingly, the performance improvement that arises from the addition of ethyl acetate, brings the PCE of devices fabricated with recrystallised FAI in line with that of those fabricated with as-received FAI from supplier A. This finding is consistent with previous studies, which have reported that the use of ethyl acetate, either as an anti-solvent[31] or as an additive to the perovskite precursor ink[32] can improve thin-film quality through improving crystallisation, and passivating defects. In contrast, the addition of 1–5 vol% isopropanol to the precursor ink does not significantly affect device performance (see Fig. S12). However, the device performance begins to decline when the IPA concentration is increased to 10 vol%. As

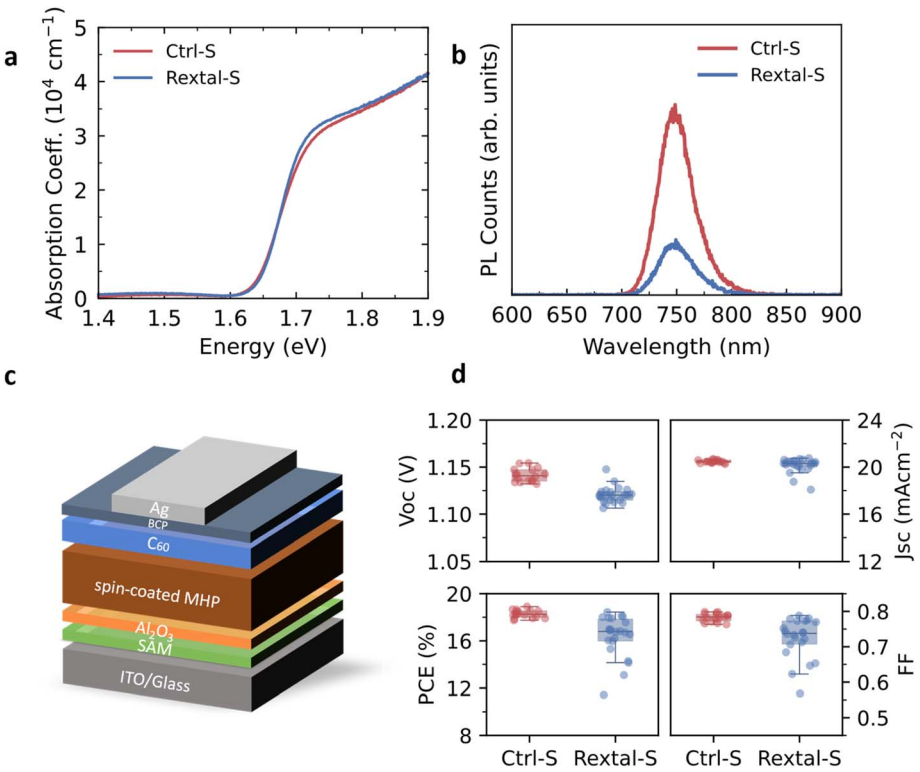

Fig. 2 Characterisation of solution-processed $FA_{0.83}Cs_{0.17}Pb(I_{0.8}Br_{0.2})_3$ MHP films and devices, made using as-received FAI (labelled as 'ctrl-S' in the figure) and recrystallised FAI (labelled as 'rextal-S' in the figure). (a) Absorption coefficient and (b) steady-state PL spectra of solution-processed $FA_{0.83}Cs_{0.17}Pb(I_{0.8}Br_{0.2})_3$ MHP films fabricated with as-received and recrystallised FAI. (c) Schematic of device architecture. (d) Performance parameters of $FA_{0.83}Cs_{0.17}Pb(I_{0.8}Br_{0.2})_3$ perovskite devices fabricated with as-received and recrystallised FAI. In the box plots, the central line inside each box represents the median value of the dataset. The box edges (lower and upper sides) indicate the first quartile (Q1) and third quartile (Q3), corresponding to the 25th and 75th percentiles, respectively. The whisker extends from the box to the smallest and largest data points within 1.5 times the interquartile range (IQR) from Q1 and Q3. Data points lying outside of this range are plotted individually as outliers.

such, it is very likely that the decrease in device performance which we see upon recrystallisation of the FAI, is a result of the removal of ethyl acetate.

To further evaluate whether the organic impurities present in FAI influence the long-term stability of solution-processed MHP, we conduct aging tests on both ctrl-S and rextal-S films at 70 ± 5 °C under 0.76-sun illumination (Fig. S13). Compared to ctrl-S films, rextal-S films exhibit slightly but not significantly faster degradation over a 95 h period. The evolution of the stabilised efficiency of unencapsulated cells aged at 70 ± 5 °C under 0.76-sun illumination in the ambient atmosphere (Fig. S14) shows similar degradation rates across all devices. This suggests that impurities in FAI do not substantially influence the stability of solution-processed MHP films under combined light and heat stressors.

Influence of FAI impurities on vapour-deposited MHP films and devices

We have now established that organic impurities in FAI, specifically trace amounts of ethyl acetate, have a positive impact on the optoelectronic properties of solution-processed perovskite thin films and devices. For simplicity, to test whether this holds true for vapour-deposition approaches, we fabricate $FAPbI_3$ MHP films and devices using dual-source co-evaporation with both as-received and recrystallised FAI from supplier A (abbreviated as 'ctrl-V' and 'rextal-V' respectively) and present the results below. In line with our previous work, to avoid confounding effects due to the surface-dependent adsorption of alkylammonium halides, we precoat our substrates with a templating layer, thus decoupling the crystallisation of perovskite from the influence of the substrate (optimisation process and evaporation details are given in the SI; Table S2 and Fig. S15–S16).[9] Interestingly here, we note that the absorption profile and coefficient of rextal-V films (Fig. 3a) is consistent with that of previously reported vapour-deposited $FAPbI_3$ films of the same composition;[29] however, the absorption coefficient is significantly higher than that of ctrl-V films. This suggests that for films of nominally the same thickness, in the case of the ctrl-V films, the precursors only partially react to form the desired photoactive (α-) perovskite phase. We note here that the electronic bandgap of both films is 1.56 eV as determined through an Elliott fit (Fig. S17). Additionally, ctrl-V films exhibit lower PL intensity than rextal-V films (Fig. 3b), while time-resolved PL measurements yield similar charge-carrier dynamics in ctrl-V and rextal-V films (Fig. S18). In light of the lower absorption coefficient (Fig. 3a), we postulate that

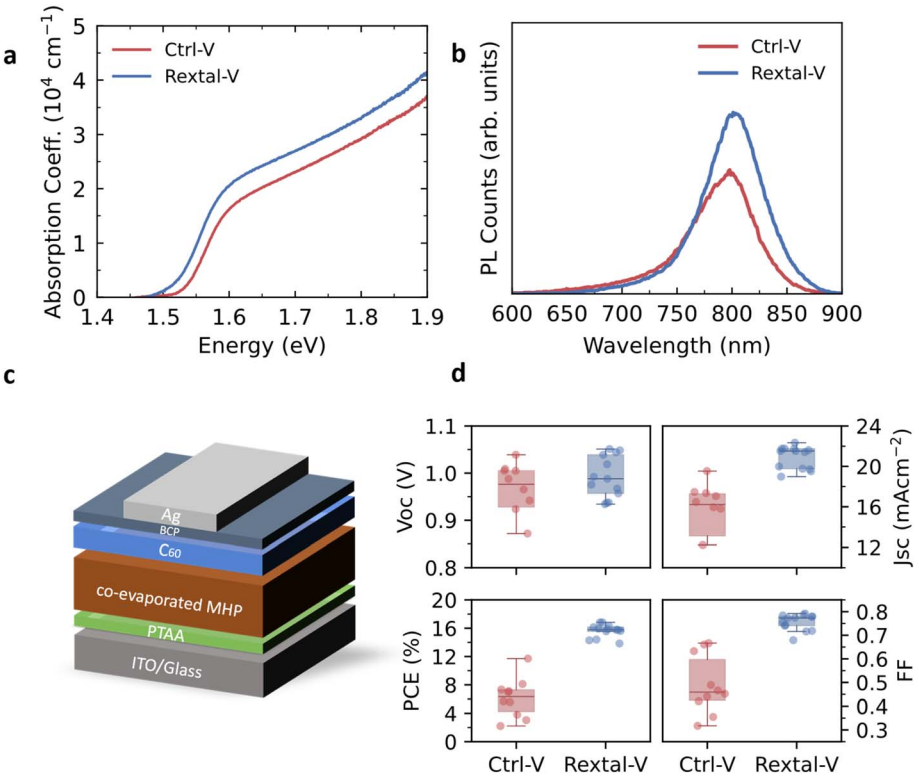

Fig. 3 Characterisation of vapour-deposited $FAPbI_3$ MHP films and devices, made using as-received FAI (labelled as 'ctrl-V' in the figure) and recrystallised FAI (labelled as 'rextal-V' in the figure). (a) Absorption coefficient and (b) steady-state PL spectra of vapour-deposited $FAPbI_3$ MHP films fabricated with as-received and recrystallised FAI. (c) Schematic for the vapour-deposited device architecture. (d) Performance parameters of $FAPbI_3$ perovskite devices fabricated with as-received and recrystallised FAI. In the box plots, the central line inside each box represents the median value of the dataset. The box edges (lower and upper sides) indicate the first quartile (Q1) and third quartile (Q3), corresponding to the 25th and 75th percentiles, respectively. The whisker extends from the box to the smallest and largest data points within 1.5 times the interquartile range (IQR) from Q1 and Q3. Data points lying outside of this range are plotted individually as outliers.

fabricating films with as-received FAI results in the formation of less photoactive perovskite for the same total film thickness.

We then incorporate these vapour-deposited $FAPbI_3$ films into p-i-n solar cells (Fig. 3c). For devices made using rextal-V films (Fig. 3d and S19), we see an increase in the average PCE from 6.2 ± 2.8% to 15.6 ± 0.9% as compared to the ctrl-V devices (further details in Table S4 and Fig. S20, S21). After purification, our co-evaporated devices achieve higher performance than previously reported values under similar conditions (Table S3). In this case, the performance enhancement is mainly due to an increase in the short-circuit current density (J_{sc}) and FF (Fig. S22). This increase in photocurrent is consistent with the higher absorption coefficient of rextal-V films.

We note that recrystallisation of the FAI results in opposite trends in solution- and vapour-processed perovskite films and devices. For solution-processing, trace impurities improve film and device quality, while for vapour-processing, they cause a marked decrease in performance. Overall, this suggests that the same impurities play very different roles in the solution-processing of MHP films than they do in vapour-processing.

Phase impurity in vapour-deposited MHP films

To probe the underlying cause of the performance enhancement which we observe in vapour-deposited MHP devices fabricated using rextal-V films, we conduct a more detailed analysis of the optical and structural properties of these films. From the absorption spectra (Fig. 4a and b), ctrl-V films exhibit more pronounced above-bandgap absorption features compared to rextal-V films. Previous studies have associated such features with the presence of hexagonal polytypes in perovskite films.[33,34] To investigate whether this is the case here, we perform XRD measurements on ctrl-V and rextal-V films (Fig. 4c and d). The diffraction pattern of ctrl-V films exhibits a broad and increased background intensity in the low-angle region ~11°–13°, where reflections from lower-symmetry polytypes of $FAPbI_3$ are typically observed. Further analysis reveals a weak, yet reproducible feature at ~11.6° (Fig. S23). Taken in conjunction with the absorption data, these observations are consistent with the presence of nanoscale regions of polytypes in ctrl-V films. While we cannot explicitly rule out the presence of higher-order hexagonal polytypes or amorphous, disordered phases (both of which would result in a lower absorption

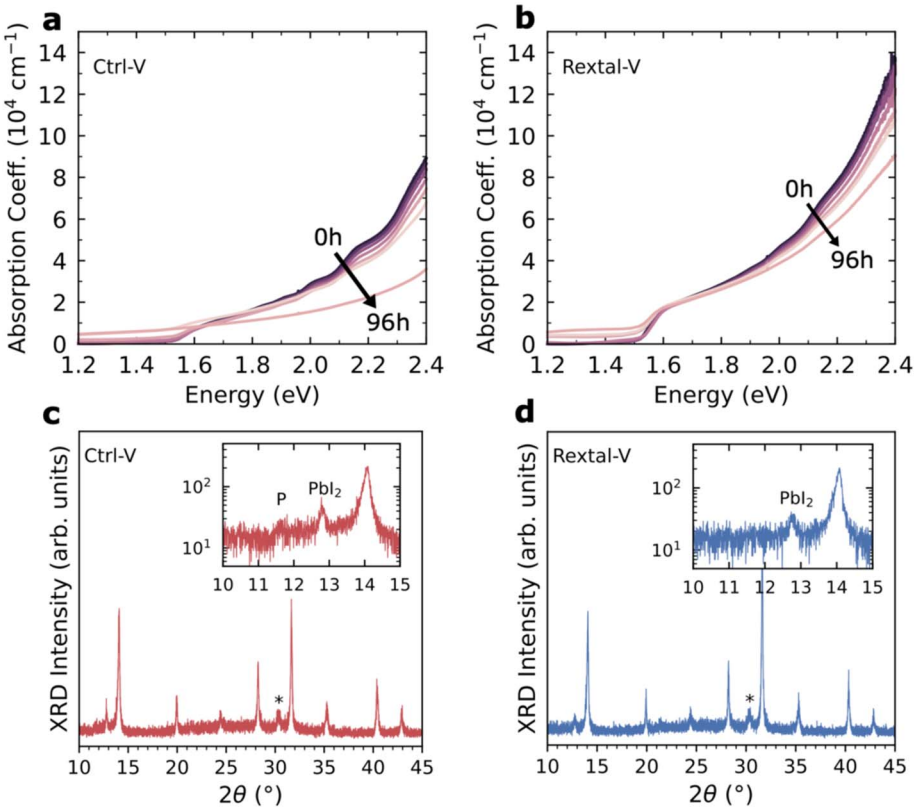

Fig. 4 Stability and structural characterisation of vapour-deposited $FAPbI_3$ MHP films made using as-received FAI (labelled as 'ctrl-V' in the figure) and recrystallised FAI (labelled as 'rextal-V' in the figure). (a and b) The absorption coefficient spectra of ctrl-V and rextal-V films aged at 70 ± 5 °C under 0.76-sun illumination in ambient atmosphere from 0 h to 96 h. (c and d) X-ray diffraction patterns of ctrl-V and rextal-V films. XRD signal from polytype (labelled as 'P' in the figure) is only identified in ctrl-V films (inset).

coefficient in ctrl-V films), these results appear to be consistent with the formation of 4H-like polytypes. Other studies have suggested that the appearance of the high-energy absorption features is due to the presence of intrinsic quantum confinement in $FAPbI_3$.[35–37] Nevertheless, irrespective of their precise origin, these high-energy absorption features have been inextricably linked to reduced device performance,[38] a phenomenon which we also observe in the present work. Indeed, when we subject ctrl-V and rextal-V films to elevated temperature and illumination (at 70 ± 5 °C under 0.76-sun illumination, unencapsulated films in ambient atmosphere), ctrl-V films suffer far more severe degradation over a 96 h period (Fig. 4a and b), consistent with the device-level stability results (Fig. S24). This agrees with literature reports which show that the presence of lower dimensional polytypes has a detrimental effect on the thermal stability of FA-based MHP films and devices.[38,39]

Impurity-related degradation process of FAI during vapour deposition

Thus far, we have established that thermally evaporated MHP films deposited with as-received and recrystallised FAI possess different optoelectronic and structural properties. However, it is still unclear how this arises from the presence of impurities in FAI. One could imagine that given the volatile nature of these organic impurities, they should readily evaporate under high-vacuum conditions, and hence not be incorporated into vapour-deposited perovskite films. Nevertheless, if the presence of volatile impurities can change the sublimation behaviour of FAI, or the rate at which it decomposes, it is conceivable that their presence can have a significant impact on the quality of the resulting perovskite films.

In vapour deposition, mass spectrometry is an effective technique with which one can analyse the chamber atmosphere during the evaporation process. By tracking the distinguishable mass-to-charge ratio (m/z) of major molecular fragments produced during the perovskite deposition, we can identify whether the impurities are evaporated along with the FAI, or if (and how) they alter the sublimation behaviour of FAI itself. Previous studies have found that upon heating, FAI undergoes several chemical reactions (Fig. 5a). Firstly, FAI ($CH(NH_2)_2I$) undergoes a reversible thermal decomposition forming formamidine ($HC(=NH)NH_2$) and hydroiodic acid (HI). Following this, there are two possible pathways for formamidine to further react. It can decompose into hydrogen cyanide (HCN) and ammonia (NH_3) (another reversible reaction), or it can react to form *sym*-triazine ($(HCN)_3$) and NH_3.[30,40]

We note here a recent study by Kuba *et al.* which explored the possibility of directly synthesising FA-based perovskites using *sym*-triazine, ammonia and HI (contradicting the irreversibility

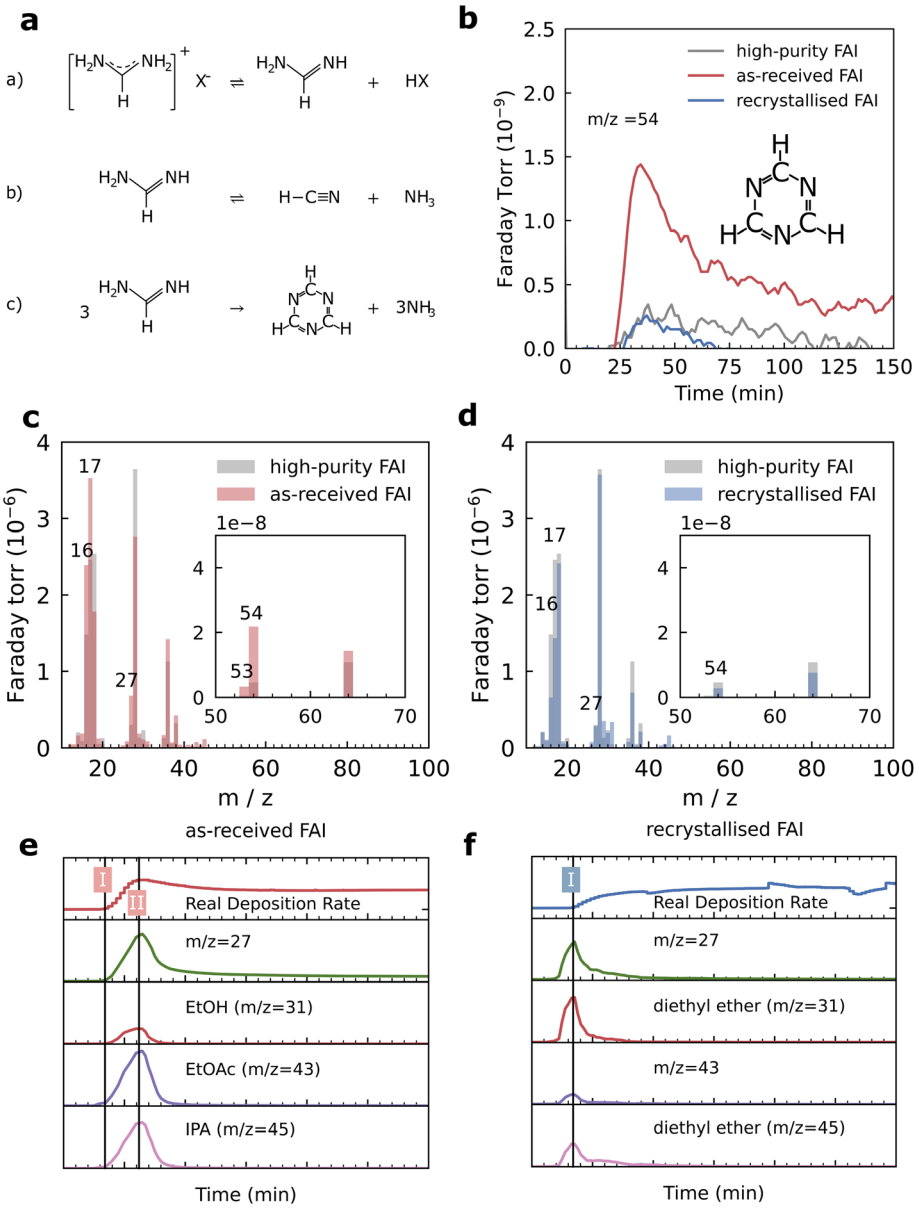

Fig. 5 The impact of impurities on evaporation behaviours and corresponding degradation process in as-received FAI, recrystallised FAI and high-purity FAI. (a) Scheme of FAI degradation reactions. (b) Mass spectra tracking of *sym*-triazine (the decomposition product of FAI, with the major *m*/*z* value of 54) during the vapour deposition. (c) Comparison of the cracking pattern of as-received FAI (red) and high-purity FAI (grey). (d) Comparison of the cracking pattern of recrystallised FAI (blue) and high-purity FAI (grey). The integration window for all cracking patterns shown in (c) and (d) is 20 cycles of the RGA scan, corresponding to an acquisition time of approximately 30 min. (e) Evaporation parameters and mass spectra tracking of as-received FAI during the vapour deposition. Line I represents the time point at which the real deposition rate begins to increase, coinciding with the initial rise in the main MS signals of ethanol (EtOH) ($m/z = 31$), ethyl acetate (EtOAc) ($m/z = 43$), and isopropanol (IPA) ($m/z = 45$). Line II labels the time point at which the real deposition rate reaches its maximum value, aligning with the peak intensities of the MS signals for impurities. (f) Evaporation parameters and mass spectra tracking of recrystallised FAI during the vapour deposition. Line I represents the time point at which the real deposition rate begins to increase, coinciding with the time point at which the main MS signals of diethyl ether ($m/z = 31, 45$) reach their maximum values.

of *sym*-triazine formation).[41] Indeed, initial work by Grundmann *et al.* discussed the reversibility of the decomposition of formamidinium chloride to *sym*-triazine, but noted that the equilibrium of this reaction sits so far to the right, that the reverse reaction is 'far from being quantitative'.[42] As such, and with consideration of the high volatility of *sym*-triazine, particularly under high-vacuum conditions, we regard the decomposition of formamidine into *sym*-triazine and NH_3 here as 'effectively irreversible'. Table S5 lists the *m*/*z* ratios of FAI and the fragments of its major thermal degradation products. Compared with the standard mass spectra of impurities (Fig. S25), we see that some of the peaks of common FAI degradation products overlap with the signals from the impurities. For example, all of the impurities identified (isopropanol,

ethyl acetate, ethanol, diethyl ether) have a signal at $m/z = 27$, which is also assigned to a major fragment peak of HCN. Given that the impurities begin to evaporate at a lower temperature than that of the sublimation and degradation of FAI, misattributing these signals to HCN would incorrectly suggest that FAI starts to degrade before even subliming. Therefore, if we want to reconstruct an accurate chemical picture of what occurs during evaporation, it is essential to identify unique signatures for the impurities, FAI, and the FAI degradation products.

Given that under atmospheric pressure the boiling points of the impurities are generally lower than the sublimation temperature of FAI (Table S6), during thermal evaporation we expect that the signals from the more volatile impurities should dominate at lower temperatures (T < 140 °C); while at higher temperatures (150 °C < T < 180 °C) we expect stronger signals from the FAI and its degradation products. We note that preheating precursors is a commonly used 'purification' strategy in thermal vapour deposition. In literature, this process generally only lasts 10 min at 100 °C until the chamber pressure stops increasing.[43–45] Here, we find that the chamber pressure still increases after preheating as-received FAI at 100 °C for 10 min. To approximate this 'purification' strategy in our experiments, we preheat the as-received FAI at an elevated temperature for a longer time until the chamber pressure stops increasing, and as such, set our preheating conditions to 130 °C for 30 min. For a direct comparison, we cool down the preheated, as-received FAI to room temperature and then, as in a regular deposition, heat it up until the real FAI deposition rate of 0.19 Å s^{-1} (the standard deposition rate of FAI for MHP co-evaporation) is achieved. We show the resulting m/z *vs.* time contour plot in Fig. S26. During the preheating, we see stronger signals from the impurities (ethyl acetate ($m/z = 43$), ethanol ($m/z = 31$, 45), and isopropanol ($m/z = 45$)) than we do during the subsequent evaporation stage. This confirms that m/z signals at 31, 43, and 45 are primarily due to the impurities. When reheating the FAI to its sublimation temperature ($T = 177$ °C), at which we obtain the desired substrate rate of FAI for the MHP co-evaporation, a new signal at $m/z = 54$ begins to appear. Unlike the ambiguous signal at $m/z = 27$, which may originate from either impurities or HCN, none of the impurities have signals at $m/z = 54$, and as such, they can only be attributed to the major fragments of *sym*-triazine. This is supported by the corresponding parent peak signals observed at $m/z = 81$ (Fig. S27), which are consistent with the reference fragmentation patterns of *sym*-triazine (Fig. S28). While another degradation product, ammonia, has a distinct signal at $m/z = 17$, it is formed in both the reversible and 'effectively irreversible' degradation pathways of FAI. Therefore, we use the appearance of the mass spectral signal at $m/z = 54$ to indicate the point at which FAI begins to decompose into *sym*-triazine and ammonia.

Interestingly, when we reheat the FAI to its sublimation temperature ($T = 177$ °C) after preheating the source at 130 °C for 30 min, the mass spectral impurity signals ($m/z = 31$, 43, 45) still quickly increase at the beginning of evaporation and only disappear after 30 min (Fig. S26). This suggests that preheating at 130 °C for 30 min is still not enough to completely remove the impurities (ethanol, ethyl acetate, and isopropanol) from as-received FAI. Instead, here, to fully purify as-received FAI (no mass spectral signals from impurities during the evaporation, Fig. S26), we have to heat the precursor up to 177 °C for 30 min.

We have now identified specific signatures for each of the impurities, FAI, and all its major degradation products. Having attributed the signal at $m/z = 54$ to *sym*-triazine, we can use this peak as the indicator of irreversible FAI degradation, and hence analyse differences in the sublimation behaviour of as-received and recrystallised FAI (high-purity FAI from supplier B is used as a standard reference). Details of evaporation rates and conditions are outlined in the SI.

In Fig. 5b, we show the mass spectrograms of as-received and recrystallised FAI from supplier A, along with the spectrogram of high-purity FAI from supplier B. To compare different groups, in all cases, we add the same amount of FAI (approximately 1 g) before the evaporation and control the real FAI deposition rate at 0.19 Å s^{-1} during the evaporation. As compared to recrystallised and high-purity FAI, in the case of the as-received FAI, we observe significantly higher *sym*-triazine ($m/z = 54$) and ammonia ($m/z = 17$) signals in the early stages of evaporation (Fig. 5c, d and S29–S31). This indicates that as-received FAI, experiences more severe 'effectively irreversible' degradation during the evaporation process than its higher-purity counterparts (recrystallised and high-purity FAI). To assess whether the more severe degradation observed during the evaporation of as-received FAI arises from decomposition of the FAI powder in the crucible, using NMR, we probe the chemical composition of the residual high-purity FAI, recrystallised FAI, and as-received FAI powders after evaporation. Fig. S32 confirms the absence of impurities or degradation products in all three residual precursors. These results indicate that the degradation observed during evaporation of as-received FAI cannot be attributed to decomposition of the FAI powder in the crucible.[46]

To determine whether the degradation products revealed by mass spectrometry also exist in the final films, we characterise the as-deposited perovskite films (prior to annealing) using NMR (Fig. S33). For the films fabricated using as-received and recrystallised FAI, we do not detect the presence of any impurities or FAI degradation products, suggesting that either they are not incorporated into the final films, or that if they are, their concentrations are below the NMR detection limit. Previous studies have suggested that the degradation products of FAI (hydrogen cyanide, *sym*-triazine, ammonia) are too volatile to adsorb onto the substrates or produce any rate reading on the QCM during the thermal evaporation.[30] Therefore, we exclude the possible incorporation of trace *sym*-triazine in the ctrl-V films.

To further probe whether the presence of impurities changes the sublimation behaviour of FAI, we compare the mass spectral signals with the evaporation process for as-received, recrystallised and high-purity FAI (Fig. 5e, f and S29–S31). Interestingly, for as-received FAI, the point at which the deposition rates begin to increase, coincides with the initial rise in the main mass spectral signals of ethanol ($m/z = 31$), ethyl acetate ($m/z = 43$), and isopropanol ($m/z = 45$) (Fig. 5e and S29). When the deposition rates reach their maximum value, the mass spectral

signals for impurities are also at their peak intensity. These results demonstrate that the evaporation of impurities in as-received FAI produces QCM rate readings at both the source and substrate levels. In contrast, with both recrystallised and high-purity FAI, the deposition rates only increase when FAI begins to evaporate (Fig. 5f and S30–S31). Consequently, the presence of trace organic impurities in as-received FAI leads to a misinterpretation of the deposition rates, as the deposition rate includes contributions from both FAI and the impurities. As a result, the composition of co-evaporated films deviates from the target stoichiometry, preventing films from fully converting into the desired photoactive phase, which leads to the formation of non-photoactive phases and reduced device performance. Notably, the extent to which impurities perturb the formation of the photoactive phase depends on both the concentration of impurities and potentially the incorporation of additional components (*e.g.*, CsI and $PbCl_2$) during evaporation which may further alter crystallisation dynamics. While impurity levels may vary between batches or even individual precursor bottles, compositional engineering may partially suppress the formation of polytype phases, even under non-stoichiometric conditions, thereby initially masking the impact of impurities on device performance (Fig. S34).

In conclusion, we have identified the chemical nature of impurities present in a commonly used commercial FAI source, and elucidated the varied effects of these impurities in both solution- and vapour-processing of metal halide perovskite thin films and devices. While ethyl acetate, as one of the impurities, can be beneficial for the quality of solution-processed perovskite films by modulating crystallisation dynamics and result in fewer or passivated defects, for vapour-processing, the impurities lead to more severe decomposition of the precursor. Although volatile degradation products are not incorporated into the films, altered sublimation behaviour can still induce stoichiometric deviations, even under optimised conditions, promoting the formation of unwanted polytype phases. Such deviations from stoichiometry is linked to the formation of non-photoactive phases, which negatively affects the optoelectronic properties of MHP thin-films. This results in both reduced film stability and decreased solar cell performance. With perovskite photovoltaics on the cusp of widespread commercialisation, fine control over reproducibility and process robustness, particularly in 'industrially ready' techniques such as thermal vapour deposition is required. The transition from research lab to industrial-scale manufacturing places increasing emphasis on material consistency, process tolerance, and production yield. In this context, our findings demonstrate that precursor purification is not merely an additional processing step, but a practical and scalable strategy for mitigating variability, stabilising evaporation dynamics, preserving stoichiometric control, and enhancing film and device performance. More broadly, this work underscores that chemical purity at the precursor level plays an underappreciated, yet significant role in enabling the reliable, industry-compatible production of perovskite photovoltaics.

Conflicts of interest

Henry J. Snaith is a co-founder and Chief Scientific Officer of Oxford Photovoltaics, a company commercialising perovskite photovoltaics. All other authors declare no conflicts of interest.

Data availability

The data supporting this article have been included in the main text, or as part of the supplementary information (SI). The supplemetary information: detailed experimental methods and additional data and figures including; NMR, UV-Vis absorption, X-ray diffraction, time-resolved photoluminescence, mass spectrometry, and device performance and stability data. See DOI: https://doi.org/10.1039/d5el00204d.

Acknowledgements

The authors gratefully acknowledge support from the Engineering and Physical Sciences Research Council (UK) (EPSRC) (EP/V011197/1, EP/T025077/1) and the Leverhulme Trust (RPG-2022-272). S. Y. acknowledges the EPSRC National Thin Film Facility for Advanced Functional Materials (NTCF), hosted by the Department of Physics at the University of Oxford, and Dr Jin Yao and Matthew Naylor, the facility stuff for their support.

References

1 NREL Best Research-Cell Efficiencies, https://www.nrel.gov/pv/cell-efficiency.html.
2 S. D. Stranks, G. E. Eperon, G. Grancini, C. Menelaou, M. J. P. Alcocer, T. Leijtens, L. M. Herz, A. Petrozza and H. J. Snaith, *Science*, 2013, **342**, 341–344.
3 J. Lim, M. Kober-Czerny, Y.-H. Lin, J. M. Ball, N. Sakai, E. A. Duijnstee, M. J. Hong, J. G. Labram, B. Wenger and H. J. Snaith, *Nat. Commun.*, 2022, **13**, 4201.
4 H. J. Snaith, *Nat. Mater.*, 2018, **17**, 372–376.
5 N. J. Jeon, J. H. Noh, W. S. Yang, Y. C. Kim, S. Ryu, J. Seo and S. I. Seok, *Nature*, 2015, **517**, 476–480.
6 J. Zhang, J. Wu, A. Barabash, T. Du, S. Qiu, V. M. Le Corre, Y. Zhao, K. Zhang, F. Schmitt and Z. Peng, *Energy Environ. Sci.*, 2024, **17**, 5490–5499.
7 D. Zheng, F. Raffin, P. Volovitch and T. Pauporté, *Nat. Commun.*, 2022, **13**, 6655.
8 D. P. McMeekin, Z. Wang, W. Rehman, F. Pulvirenti, J. B. Patel, N. K. Noel, M. B. Johnston, S. R. Marder, L. M. Herz and H. J. Snaith, *Adv. Mater.*, 2017, **29**, 1607039.
9 S. Yan, J. B. Patel, J. E. Lee, K. A. Elmestekawy, S. R. Ratnasingham, Q. Yuan, L. M. Herz, N. K. Noel and M. B. Johnston, *ACS Energy Lett.*, 2023, **8**, 4008–4015.
10 H. Zhu, S. Teale, M. N. Lintangpradipto, S. Mahesh, B. Chen, M. D. McGehee, E. H. Sargent and O. M. Bakr, *Nat. Rev. Mater.*, 2023, **8**, 569–586.
11 Z. Shen, Q. Han, X. Luo, Y. Shen, Y. Wang, Y. Yuan, Y. Zhang, Y. Yang and L. Han, *Nat. Photonics*, 2024, **18**, 450–457.

12 T. A. Chowdhury, M. A. Bin Zafar, M. Sajjad-Ul Islam, M. Shahinuzzaman, M. A. Islam and M. U. Khandaker, *RSC Adv.*, 2023, **13**, 1787–1810.
13 L. Chen, T. Liu, H. Yu, Z. Zhang, C. Qin, N. Zhang, L. Yu, F. Yang, G. Song and Z. Liu, *J. Alloys Compd.*, 2023, **942**, 168924.
14 S. Cai, Z. Li, Y. Zhang, T. Liu, P. Wang, M.-G. Ju, S. Pang, S. P. Lau, X. C. Zeng and Y. Zhou, *Nat. Commun.*, 2024, **15**, 2329.
15 P. Zhu, D. Wang, Y. Zhang, Z. Liang, J. Li, J. Zeng, J. Zhang, Y. Xu, S. Wu and Z. Liu, *Science*, 2024, **383**, 524–531.
16 C. Zhang and N.-G. Park, *Commun. Mater.*, 2024, **5**, 194.
17 D. C. Senevirathna, J. C. Yu, T. A. Nirmal Peiris, B. Li, M. Michalska, H. Li and J. J. Jasieniak, *ACS Mater. Lett.*, 2021, **3**, 351–355.
18 M. Abdi-Jalebi, Z. Andaji-Garmaroudi, S. Cacovich, C. Stavrakas, B. Philippe, J. M. Richter, M. Alsari, E. P. Booker, E. M. Hutter and A. J. Pearson, *Nature*, 2018, **555**, 497–501.
19 M. Roß, M. B. Stutz and S. Albrecht, *Sol. RRL*, 2022, **6**, 2200500.
20 R. A. Kerner, E. D. Christensen, S. P. Harvey, J. Messinger, S. N. Habisreutinger, F. Zhang, G. E. Eperon, L. T. Schelhas, K. Zhu and J. J. Berry, *ACS Appl. Energy Mater.*, 2023, **6**, 295–301.
21 J. Borchert, I. Levchuk, L. C. Snoek, M. U. Rothmann, R. Haver, H. J. Snaith, C. J. Brabec, L. M. Herz and M. B. Johnston, *ACS Appl. Mater. Interfaces*, 2019, **11**, 28851–28857.
22 Z. Yang, J. Dou, S. Kou, J. Dang, Y. Ji, G. Yang, W.-Q. Wu, D.-B. Kuang and M. Wang, *Adv. Funct. Mater.*, 2020, **30**, 1910710.
23 H. Wen, Z. Zhang, Y. Guo, W. Luo, S. Si, T. Yin, H. Wu and S. Huang, *Adv. Energy Mater.*, 2023, **13**, 2301813.
24 X.-X. Gao, W. Luo, Y. Zhang, R. Hu, B. Zhang, A. Züttel, Y. Feng and M. K. Nazeeruddin, *Adv. Mater.*, 2020, **32**, 1905502.
25 S.-H. Turren-Cruz, A. Hagfeldt and M. Saliba, *Science*, 2018, **362**, 449–453.
26 G. E. Eperon, S. D. Stranks, C. Menelaou, M. B. Johnston, L. M. Herz and H. J. Snaith, *Energy Environ. Sci.*, 2014, **7**, 982–988.
27 C. J. Dolan, E. R. Yakel, S. Liu, R. A. Kerner, J. R. Palmer, K. X. Vences, H. M. Vossler, C. Han, S. P. Dunfield and D. P. Fenning, *J. Mater. Chem. C*, 2025, **13**, 9584–9592.
28 K. B. Lohmann, S. G. Motti, R. D. J. Oliver, A. J. Ramadan, H. C. Sansom, Q. Yuan, K. A. Elmestekawy, J. B. Patel, J. M. Ball, L. M. Herz and M. B. Johnston, *ACS Energy Lett.*, 2022, **7**, 1903–1911.
29 J. Borchert, R. L. Milot, J. B. Patel, C. L. Davies, A. D. Wright, L. M. Maestro, H. J. Snaith, L. M. Herz and M. B. Johnston, *ACS Energy Lett.*, 2017, **2**, 2799–2804.
30 M. Kroll, S. D. Öz, Z. Zhang, R. Ji, T. Schramm, T. Antrack, Y. Vaynzof, S. Olthof and K. Leo, *Sustain. Energy Fuels*, 2022, **6**, 3230–3239.
31 W. Zhang, Y. Li, X. Liu, D. Tang, X. Li and X. Yuan, *Chem. Eng. J.*, 2020, **379**, 122298.
32 P. Zhang, N. Gu, L. Song, X. Chen, P. Du, L. Zha, W.-H. Chen and J. Xiong, *Nanoscale*, 2022, **14**, 5204–5213.
33 G. Bravetti, N. Taurisano, A. Moliterni, J. M. Vicent-Luna, D. Altamura, F. Aiello, N. Vanni, A. L. Capodilupo, S. Carallo, G. Gigli, G. Uccello-Barretta, F. Balzano, C. Giannini, S. Tao, S. Colella and A. Rizzo, *Chem. Mater.*, 2024, **36**, 3150–3163.
34 P. Gratia, I. Zimmermann, P. Schouwink, J.-H. Yum, J.-N. Audinot, K. Sivula, T. Wirtz and M. K. Nazeeruddin, *ACS Energy Lett.*, 2017, **2**, 2686–2693.
35 A. D. Wright, G. Volonakis, J. Borchert, C. L. Davies, F. Giustino, M. B. Johnston and L. M. Herz, *Nat. Mater.*, 2020, **19**, 1201–1206.
36 K. A. Elmestekawy, B. M. Gallant, A. D. Wright, P. Holzhey, N. K. Noel, H. J. Snaith, M. B. Johnston and L. M. Herz, *ACS Energy Lett.*, 2023, **8**, 2543–2551.
37 D. Guo, T. A. Selby, S. Kahmann, S. Gorgon, L. Dai, M. Dubajic, T. C.-J. Yang, S. M. Fairclough, T. Marsh, I. E. Jacobs, B. Wu, R. Guo, S. Nagane, T. A. S. Doherty, K. Ji, C. Liu, Y. Lu, T. Kang, C. Mamak, J. Mao, P. Müller-Buschbaum, H. Sirringhaus, P. A. Midgley and S. D. Stranks, *Nat. Nanotechnol.*, 2025, **20**, 1771–1778.
38 H. Liu, B. Zheng, X. Wang, W. Ning, L. Wan, Y. Wang and T. Liu, *Adv. Funct. Mater.*, 2025, **35**, 2425620.
39 S. Li, J. Xia, Z. Wen, H. Gu, J. Guo, C. Liang, H. Pan, X. Wang and S. Chen, *Adv. Sci.*, 2023, **10**, 2300056.
40 E. J. Juarez-Perez, L. K. Ono and Y. Qi, *J. Mater. Chem. A*, 2019, **7**, 16912–16919.
41 A. G. Kuba, F. Sahli, M. Othman, K. Artuk, Q. Jeangros, A. Hessler-Wyser, C. Ballif and C. M. Wolff, *ACS Energy Lett.*, 2025, **10**, 2710–2717.
42 C. Grundmann and R. Ratz, *J. Org. Chem.*, 1956, **21**, 1037–1038.
43 B.-S. Kim, L. Gil-Escrig, M. Sessolo and H. J. Bolink, *J. Phys. Chem. Lett.*, 2020, **11**, 6852–6859.
44 T. Abzieher, D. T. Moore, M. Roß, S. Albrecht, J. Silvia, H. Tan, Q. Jeangros, C. Ballif, M. T. Hoerantner and B.-S. Kim, *Energy Environ. Sci.*, 2024, **17**, 1645–1663.
45 D. M. Mattox, *Handbook of Physical Vapor Deposition (PVD) Processing*, William Andrew, 2010.
46 J. Petry, V. Škorjanc, A. Diercks, T. Feeney, A. Morsa, S. R. Kimmig, J. Baumann, F. Löffler, S. Auschill, J. Damm and D. Baumann, *EES Sol.*, 2025, **1**, 404–418.

